Title: Soft dielectric elastomer oscillators driving bioinspired robots

Authors: E.-F. Markus Henke[1,2,*], Samuel Schlatter[3], Iain A. Anderson[1,†]

Affiliations:

[1] Auckland Bioengineering Institute, The University of Auckland, 70 Symonds Street, Auckland, New Zealand

[2] Solid State Electronics Institute, TU Dresden, Dresden, Germany

[3] Microsystems for Space Technologies Laboratory, Ecole Polytechnique Fédérale de Lausanne, Lausanne, Switzerland

Correspondence to: *m.henke@auckland.ac.nz, †i.anderson@auckland.ac.nz

Abstract: Entirely soft robots with animal-like behavior and integrated artificial nervous systems will open up totally new perspectives and applications. To produce them we must integrate control and actuation in the same soft structure. Soft actuators (e.g. pneumatic, and hydraulic) exist but electronics are hard and stiff and remotely located. We present novel soft, electronics-free dielectric elastomer oscillators, able to drive bioinspired robots. As a demonstrator we present a robot that mimics the crawling motion of the caterpillar, with integrated artificial nervous system, soft actuators and without any conventional stiff electronic parts. Supplied with an external DC voltage, the robot autonomously generates all signals necessary to drive its dielectric elastomer actuators, and translates an in-plane electromechanical oscillation into a crawling locomotion movement. Thereby, all functional and supporting parts are made of polymer materials and carbon. Besides the basic design of this first electronic-free, biomimetic robot we present prospects to control the general behavior of such robots. The absence of conventional stiff electronics and the exclusive use of polymeric materials will provide a large step towards real animal-like robots, compliant human machine interfaces and a new class of distributed, neuron-like internal control for robotic systems.

MAIN TEXT:

Introduction:

The vast majority of soft robots use pneumatic (*1-3*) or hydraulic (*4*) actuators. They can be made to operate in multi-freedom motion by using joined multiple chambered segments. A four-legged crawling robot by Shepherd et al. (*3*) can move under the separate pneumatic actuation of each leg. In another instance an octopus-arm actuator can be steered using tendon-like cords (*5*). The bulk of active elements in soft biomimetic robots are compliant materials like silicone or natural rubber with low Young's moduli, in the order of 10^4-10^9 Pa, that compare well to the moduli of biological materials (*6*). Conventional robot motors, gears and fixtures are orders of magnitude stiffer, and built from materials with moduli in the range 10^9-10^{12} Pa (*6, 7, 8*). But whether they are hard or soft, the majority of actuators require external power and control units composed of dense electronic components on stiff printed circuit boards that are remotely located from the actuator. Thus, soft robotic actuators can never be entirely soft in a complete assembly of actuator

and controller, if they rely on electronic control and software algorithms. The integration of sensory functionalities into soft structures is even more challenging. Although there are promising developments in flexible and stretchable electronics (*9*) and miniaturization of electronics enables small signal-processing-, control- and sensor nodes, conventional electronics will always rely on silicon-semiconductor technologies and be orders of magnitudes stiffer than so-called soft materials. Therefore, an integration of conventional electronic components introduces stiff areas in an otherwise soft design. To emulate entirely soft machinery, we need a technology that is soft, fully autonomous and capable of self-regulation without conventional hard electronics. A promising development in that direction is the integration of microfluidic logics (*10*) based on monopropellant fuels, that decompose into gas and power pneumatic robots (*11*). The 'octobot' presented by Wehner et al. (*12*) represents a first entirely soft, autonomous robot using these technologies. The difference to other actuation technologies here is, that the source of actuation cannot be influenced by established control algorithms. Although the usage of monopropellant fuels represent one pathway to entirely soft robots, we believe that the usage of electronically active smart materials is advantageous.

Within the range of smart actuator technologies, there is one with mechanical characteristics similar to biological muscle (*13*): the dielectric elastomer actuator (DEA) (*14*), a sub-type of soft polymeric actuators, so-called electroactive polymers, well known for their robotic applications (*15*). Its mechanism is electro-mechanical, offering the opportunity for rapid and fully integrated control of actuation. In its simplest embodiment a DEA is a flexible capacitor consisting of a thin, pre-strained, material such as acrylic or silicone rubber. A membrane of typically 50 μm thickness is flanked on both sides by a stretchable electrode (Fig. 1A). Application of charge to the electrodes produces an electrostatic Maxwell pressure, resulting in in-plane expansion and across-thickness contraction (Fig. 1B) (*16*). With impressive operating capabilities that include maximum areal strains in excess of 1692% (*17*), DEA can be made to match and exceed the performance of natural muscles, earning the moniker of artificial muscles (*18*). In addition to being used as actuators with large actuation (*13, 16, 17*), DE devices can perform as sensors for large strain (*19, 20, 21*) (Fig. 1C) and as energy harvesters (*22, 23*) (Fig. 1D). Some of these functions can be combined in a single assembly (*14*). For instance, DEAs, made touch sensitive through electronic capacitive sensing, can be placed in arrays so that they autonomously push an object forward, mimicking the mechanosensitive actuation of cilia (*24*). Besides all the advantageous characteristics, DEs in general have one major drawback. While sensing mainly works with low voltage, actuation and energy harvesting require high voltage of up to several thousand volts. This issue is problematic for biomedical applications and can cause problems in wet environments. There are current developments to solve these problems and lower the necessary voltage by decreasing the layer thickness of DE membranes (*25, 26*) or chemically tailoring the used silicones in order to increase the dielectric constant (*27*).

One way to achieve localized self-regulated DEA charge control is to use strain directly as a means for electronic charge switching. A piezo-resistive material is required for this, one that can undergo large changes in resistivity, under a realistic actuation strain. Beruto et al. demonstrated that stretchable materials, such as silicon-graphite mixtures, show large changes in piezoresistivity (in the order of 10^5) at low voltages, with strains on the order of 10%, around the percolation threshold. They went on to suggest that such piezoresistivity can provide a means for strain and pressure sensing (*28*). O'Brien et al, showed that piezoresistivity can also be used for

strain controlled electronic switching (*29*). For this to work with DEA the switching behavior would need to operate within the kilovolt range of DE.

O'Brien et al. (*29*) identified a suitable high-voltage switching material, consisting of carbon particles in silicone grease, that can be imprinted on the membrane surface or alongside a DEA: the dielectric elastomer switch (DES). The conductivity of a DES will change by several orders of magnitude through a voltage-induced elongation of an adjacent DEA (*29*). DEAs and DESs can be combined together as strain-dependent electrical signal inverters. When an odd number of these inverters are assembled in a closed loop cycle, one obtains a soft electro-mechanical oscillator that is entirely and uniquely controlled by elastomer strain (*30*), without any conventional electronic components being used. This inverter provides a basis for periodic charge control; emulating the role of a biological central pattern generator (CPG) neural network.

To demonstrate the potential use of the mechanosensitive DEA/DES oscillator for soft, self-controlled robots without conventional, stiff electronics, we have designed a robot that mimics a crawling motion similar to a caterpillar or an inchworm. All necessary actuators, signal processing and circuitry are composed solely of elastomers, PMMA and imprinted or brushed carbon electrodes (Fig. 2B). The mechanism is a combined mechano-electronic oscillator/crawling machine that operates without the need for an external control signal (Fig. 2B). The robot 'Trevor' generates its driving signals using a DEA/DES oscillator that serves as a timing mechanism and a muscle-drive for its feet. The generated phase-shifted signals cause six DE actuator muscles to move five pairs of feet in a cyclic crawling motion. The energy source for this is an external DC voltage supplied through live copper tracks in contact with the feet.

Similar to caterpillars that possess three pairs of stiff jointed thoracic legs, two to five pairs of soft abdominal legs – the so-called prolegs - and one pair of terminal prolegs at the last body segment (Fig. 2A), our demonstrator robot possesses six body segments equipped with legs. A crawling motion in caterpillars is generated by a series of phase-shifted steps in the individual body segments equipped with prolegs. Muscles in each segment cause the segment and its proleg to lift, move forward and settle again. Starting at the end these single steps in each proleg cause the caterpillar to move forward. A biomimetic crawling motion is also generated by our demonstrator robot.

Materials and Methods

Dielectric elastomer oscillators with tunable oscillation frequencies

The fundamentals of a dielectric elastomer oscillator (DEO) were demonstrated by O'Brien et al.; in (*29*) they presented dielectric elastomer switches (DESs) and in (*30*) the dielectric elastomer oscillator (DEO). DESs are piezoresistive electrode areas on DE membranes, able to change their electrical resistance and switch charge flow on and off upon a mechanical deformation. The first DESs could change their electrical resistance R_{DES} by three orders of magnitude and were used in basic digital units such as inverters and NAND gates. A new production technology presented here, enables improved DES and inverters that enable DES with controllable oscillation frequencies and a lifetime of more than 20,000 oscillation cycles.

A dielectric elastomer inverter consists of a DEA combined with a DES, both arranged side by side, on the same elastomer membrane. In its initial state (Fig. 3A), a low input voltage signal (V_{in}<1000 V) is applied to its signal input. That voltage signal is too low to significantly actuate the DEA and, hence, the actuator does not compress the piezoresistive DES track sufficiently to

switch it to its conductive mode. The DES possesses a high electrical resistance of $R_{DES}>10^{12}\Omega$ which forces the output signal V_{out} to a high voltage signal. DESs used in this study can change resistance by at least six orders of magnitude (Fig. 3C). By applying a high voltage signal to the input, the DEA actuates, compressing the DES, and causing its resistance and output voltage to drop (Fig. 3B). The inverters work reliably (Fig. 3D) over several thousand cycles and can be assembled to form all basic Boolean logic gates (*31*).

As already presented in (*30*), a closed loop of an uneven number of inverters represents a self-oscillating DEO. O'Brien et al. assembled three DE NAND gates in a closed loop, connecting the first input to a high supply voltage. The output of every NAND stage was connected to the input of the next stage and the last output to the first input. The presented oscillator then behaved as a three stage inverter oscillator and showed a stable, nearly rectangular, oscillation between the low and high signal level at approximately 1Hz with a lifetime of about 180 cycles. The frequency of such an oscillator depends on so-called propagation delay. This is the time a single stage needs to change its output signal level when the input signal changes. In a DEO that time is mainly dependent upon the charging speed and viscoelastic losses in the DEAs. The original design does not possess electrical elements with controllable values and, therefore, will always oscillate with a constant oscillation frequency.

To reduce complexity, enable a frequency control and increase the overall lifetime, a new production technology for DEOs was developed and, instead of NAND gates (*30*), simple DE inverters were used. This halved the required number of DEAs and DESs, reducing the DE parts that can fail, thus improving the system reliability. Fig. 4 depicts the original design (4B) presented in (*30*) with the new design (4B). The newly introduced series resistors replace the upper half of every NAND gate (*31*), define the time constant for charging the capacitors of the individual DEAs and, hence, the propagation delay of every stage. The oscillation frequency is, according to Mandal et al. (*32*), proportional to the inverse of twice the sum of the individual propagation delays of all inverter stages. The oscillation frequency can therefore be set by tuning the series charging resistors:

$$f_0 = \frac{1}{2n\tau_d}, \tag{1}$$

$$\tau_d \propto R_S, \tag{2}$$

$$f_0 \propto \frac{1}{R_S}. \tag{3}$$

Where f_0 is the oscillation frequency of the oscillator, n the number of inverter stages, τ_d the propagation delay of a single stage and R_S the series resistor.

Functionality of an electronics-free dielectric elastomer oscillator

An idealized electrical model of the DEO and its electromechanical states, during an entire oscillation cycle with periodic time $T=t_1+t_2+t_3$, is depicted in Fig. 5. The dielectric components (left representations) can be modeled with electrical components (middle representations). The DEA act as capacitors C_1, C_2 and C_3, the switches as variable resistors R_{DES1}, R_{DES2} and R_{DES3} and the series charging resistors as constant resistors R_{S1}, R_{S2} and R_{S3}. After applying a supply voltage

V_S to the oscillator, a self-primed oscillation, with three phase shifted voltages dropping over the individual inverters, is generated. The phase shift between the voltage signals is φ=120°. After a settling time the voltage signals oscillate with constant amplitude and frequency. The maximum voltage on a fully charged capacitor travels from DEA 3 to the left to DEA 1 and starts again from DEA 3. In Fig. 5A at t_1 the capacitor representing DEA 3 is fully charged, capacitor DEA 2 is being charged and DEA 1 is being discharged. The maximum voltage at DEA 3 causes the maximum elongation of DEA 3 and compresses DES 3. This switch then acts as a conductor and discharges the capacitor DEA 1. This actuator shrinks to its initial shape and switches DES 1 off (i.e. high resistance state). The absence of a conduction path along DES 1 forces the current through R_{S1} to charge the capacitor DEA 2. The increasing charge on DEA 2 causes that actuator to elongate and simultaneously lowers the resistance of DES 2. That leads to the discharge of capacitors DEA 3 via DES 2. After the first third of a cycle (T/3) at t_2 (Fig. 5B) the voltage on DEA 2 reaches its maximum value. Therefore, DES 2 is conducting and discharges capacitor DEA 3. The switch DES 3 now returns to its high resistance state, causing the current through R_{S3} to charge capacitor DEA 1. After two thirds of a cycle (2T/3) at t_2 DEA 1 is fully charged, the switch DES 1 is conducting, discharges DEA 2 and DEA 3 starts charging again (Fig. 5C) - restarting the overall cycle. As result, a continuous, self-primed, electro-mechanical, travelling wave from right to left is generated.

Production of the dielectric elastomer components

The physical design of a fully integrated dielectric elastomer oscillator is shown in Fig. 6. All necessary components are arranged on the same pre-strained DE membrane that is held by a laser cut PMMA frame. Every DEA is located next to a DES. That makes three inverters (Fig. 6 B) that are connected in series in a closed loop. The series resistors are applied to the PMMA frame.

The Dielectric Elastomer Actuators (DEAs) and Dielectric Elastomer Switches (DESs) used in the electronic-free DEOs are applied to a pre-strained VHB 4905 (by 3M) membrane. To ensure proper functionality of the actuators and the switches, both components require different, and specific, membrane pre-strains and, therefore, are applied in individual steps (Fig. 7).

To produce the DE membrane, a piece of VHB 4905 is supported in an iris-like device and pre-strained to intermediate pre-strain of λ=1.9 (Fig. 7 A-B). A support frame, to hold the pre-strained DE membrane, is also laser cut using a Trotec Speedy 300; simultaneously the locations for the carbon grease resistors are engraved. Afterwards, Nyogel 756G carbon grease is applied to the resistor tracks using a brush and the surplus grease is removed with a wipe.

At that pre-strain the switching tracks are applied to the membrane by an imprint process. The switching grease, consisting of a 5:1 mixture by weight of Molykote 44 Medium grease to Cabot Vulcan XC72 carbon, is applied to a PDMS stamp (Sylgard 184, by Dow Corning) using a size zero soft taper point color shaper from Royal Sovereign Ltd. UK. The coated stamp is then pressed on the top of the membrane, against a flat counter mold from the bottom of the membrane, for at least 30 seconds to ensure a proper transfer of the switching grease. The above procedure is repeated for all necessary switches. The selected carbon grease is conductive in that composition and has to be further pre-strained to decrease the carbon concentration below percolation. To do so, the membrane is further strained to a final pre-strain of λ=3.5. That yields a pre-strain in the switch of approximately 1.85 (Fig. 7 C).

After pre-straining the membrane, the prepared PMMA frame is applied to it from the bottom. During this step, it has to be ensured, that the membrane and the frame are positioned accurately with respect to each other. To ensure a proper switching by the DES, the individual DES have to be placed as near as possible to the adjunct frame edge (Fig. 7D). For an uniaxial compression of the individual switches, narrow PMMA stiffener bars are also attached to the membrane from underneath (Fig. 7 D). Finally, the electrodes for the DEAs are hand brushed to the membrane using Nyogel 756G carbon grease and all necessary conductive tracks are hand brushed onto the top and the bottom of the assembled DEO.

Design of autonomous, electronics-free, bioinspired demonstrator robot Trevor

Trevor (Fig. 8A) is built up from polymer materials and carbon. His body is structured in six body segments equipped with legs, similar to a caterpillar. To transform the in-plane oscillating movement of the integrated DE muscles into a forward locomotion each body segment of the robot is equipped with its own DEA. The last three segments represent a fully integrated DEO as active signal generator. Each of the 3 oscillator DEAs is wired in tandem to a 'slave' muscle, further forward along the array, bringing the total number of actuators to 6. The phasic in-plane motion of the 6 DEAs is translated into a forward motion through five V-shaped compliant legs, laser cut from 127µm thick PET film (Duralar .005). Thus, each leg connects two adjacent DEAs (Fig. 8B). Although the skeletal frame is made of PMMA (Y=1.8…3.1x10^9 Pa), a relatively stiff material, the functional components, such as the biomimetic signal generator and the DE actuators, are comprised of much softer materials; a first step towards an electronics-free fully soft robot. In the next development step the remaining stiff materials will be replaced by soft silicone elastomers too. The overall length is 250 mm, with width 80 mm.

If one DEA is activated, it elongates and the elastomer membrane in the corresponding body segment loses tension; this causes the leg beneath it to move up and forward (Fig. 8C). After the DEA's full elongation, the DES network discharges this DEA and, at the same time, charges the one behind it (Fig. 8D). The first leg moves down into contact with the supporting surface while the leg behind it moves up and forward (Fig. 8E). The self-generated signal travels from actuator to actuator from the front to the back of the robot. Although this wave travels in the reverse direction, the resulting crawling motion is forward. This is due to the mounting points of the legs at the front end of each DE muscle. A full oscillation cycle, and the generated movement, is depicted in Fig. 9 schematically.

Experiments and results

Experimental set up

All experimental investigations described in this contribution were performed in the Biomimetics Lab at the Auckland Bioengineering Institute. As voltage supply, a Biomimetics EAP controller, an in-house developed, remotely controllable 4-channel high voltage signal generator (maximal 5000V at 125µA per channel) was used, remotely controlled by lab-developed LabView software application. Voltage measurements were performed with a self-developed, high-resistance voltage divider combined with a pre-amplifier to step down the high voltages to low voltage signals, which were measured by a National Instruments SCB-68 analog to digital converter unit and processed by LabView. The position of the robot and, thus, its motion were measured by a laser

distance sensor LDS70-200 by Eltrotec and also recorded and processed by LabView. Photographs were taken with a Canon EOS 70D digital single-lens reflex camera.

Signal generation and frequency control in DEOs

To demonstrate the potential of the developed electronics-free dielectric elastomer oscillators with controllable oscillation frequency, several DEOs were assembled and their voltage signals were measured. The DC input voltage was set between 3,250 V and 4,000 V, the series resistors were set between 33 MΩ and 1000 MΩ and different geometries were used. To investigate influences of different quantities on the oscillation frequency, the resistors were not integrated into the oscillator frames, but external conventional devices were used. This was due to the integrated carbon resistors being not exchangeable at the current stage of development. The generated oscillating voltages over the three inverter units V_1, V_2 and V_3 were measured by connecting the circuit nodes between the series resistors and the DESs to the voltage divider and measurement amplifier.

Fig. 10 depicts the general signal waveform generated by a three stage inverter oscillator. Fig. 10A shows measured, oscillating, voltage signals generated by a DEO with DEAs of w_{DEA}=53.5 mm width and l_{DEA}=27 mm length, the membrane thickness d_{DE}=40µm, the capacitance of the single DEAs varied from C_{DEA}=0.5nF to 4.5nF. Fig. 10B show one voltage signal for a lifetime test.

As can be seen in Fig. 10A, the signals show charging and discharging processes of capacitors (DEAs) through large resistors (R_S and R_{DES}). The frequencies depend on the values of the series charging resistors R_S. A large resistor value limits the currents that charge and actuate the DEAs and yield longer propagation delays. For small resistors higher currents flow and charge the DEAs' capacitances faster; propagation delay reduces and, hence, the oscillation frequency rises. Regarding the fact that the geometric values (w_{DEA} and l_{DEA}) of a DEO are fixed after its assembly, applying variable resistors is a suitable approach to control the frequency of DEOs. For R_S of the same resistance value, the three voltage signals are 120° phase shifted and oscillate reliably between a high and a low signal level. The signal level, thereby, depends on the ratio between the series resistors, the resistance values the individual DESs take during the oscillation and the value of leakage resistance through the DEA membranes (*33*). The maximum signal level rises if the series resistor values decrease. The low signal level depends mainly on the amount of actuation of the DEAs and, therefore, the in-plane compression of the DESs. All measurement data indicates that the low signal levels decrease over time until a fatal failure of one of the DE components occurs. This behavior can be explained by the viscoelastic behavior of the used material. It possesses a large viscoelasticity (*34*) that influences the actuation of a DEA even after several minutes. A virgin DEA does not generate as much actuation as a DEA that has run for thousands of cycles; operation time is needed for the DEAs to reach their maximum elongation and the related DESs to reach minimum resistance. Equivalently, at high frequencies the DEA does not have sufficient time to shrink to its initial length. In the next cycle, there is then residual actuation that enables the DEA to compress the DES further, which happens repeatedly per cycle until the DEA reaches an equilibrium electromechanical oscillation; the resistance and, hence, the voltage reach lower values over time and at higher frequencies.

By changing series charging resistor values, the frequency of oscillators can be tuned within the range of 20 to 36 times, depending on the input voltage level and the geometry. In general, measurements indicate that the ratio f_{max}/f_{min} is higher for DEOs possessing smaller DEAs and lower input voltages. To derive a general relation more measurements will be performed in a future study. The average ratio is 27.7 and represents a possible approach to widely tune the oscillation frequency of DEOs.

This general trend can be seen in Fig. 10B that represent a life-time evaluation of a DEO. Every oscillator needs a certain amount of time to self-start its oscillation. That process can be seen in the time segment 10-30s. In every cycle the DEAs elongate a little more and further compress the adjacent DESs; the minimum voltage signals decrease. After about 200s the signal looks stable, but the minimum signal amplitude will further decrease over time. It is to be noted that the signals reach the maximum high signal level after only a couple of cycles, that is, because the DES will reach their high resistance state even if there is residual charge and elongation of the DEA (Fig. 3C). The maximum life time that we can report so far was >30,000 cycles at 1.58Hz, with an aggregate runtime of more than five hours (Fig. 10 B).

Different influences on the signal frequencies are displayed in Fig. 11. All charts but Fig. 11B show the main possibility of frequency control by changing the charging resistor values. In Fig. 11A the voltage dependence is shown additionally. A higher supply voltage V_{In} yields higher frequencies for all R_S. In average an increase by 250V raises the frequency by 13.4% with a standard deviation of 3.2%; this behavior is independent on the series resistor values, the height of the voltage, and the DEA geometry and can be applied at any operating point. Within the used voltage range the frequency can thereby be tuned by 39% in total at any operating point within the possible operating voltages.

As discussed in the introduction, the capacitance of the DEAs also influences the oscillation frequency. Fig. 11C and Fig. 11D depict the geometry influence on oscillation frequencies in addition to the already mentioned resistance dependence. In general, all measurements point out that an increase in one geometric dimension (w_{DEA} or l_{DEA}) will decrease the oscillation frequency independently of the resistance value, if the other geometric dimension stays fixed. At this point we cannot give a general ratio per millimeter for this dependence with sufficient trust, since the DEAs were all produced by hand and the geometric dimensions are not sufficiently accurate.

The maximum operation frequencies of DEOs, of the current state of the art, are limited by the viscoelastic losses in the used membrane material and the maximum current that the switches can reliably can switch. Typically the maximum operation frequencies are between f_{max}=5…10Hz. The maximum reported frequency so far was ≈13Hz. This value is expected to increase largely by using pure elastic silicone membranes and more reliable production technologies. The maximum operation voltage is set at V_{In}=4000V for current oscillators. Higher voltages cause the switches to degrade fast. Better production technologies that enable more homogeneous DES can increase that value. Voltages above 5000V are not necessary to run most of DEs and, therefore, are not essentially a focus of further development.

However, and in summary, measurements have shown that DEOs can be designed to operate at a certain oscillation frequency f_0 by adjusting their geometry and series charging resistors R_S. Furthermore, it is possible to tune this frequency either by the applied input voltage, or a variable resistor. This opportunity will be further addressed in the discussion section.

Bioinspired crawling robot – Trevor the caterpillar

To demonstrate the capability of DEOs autonomously driving bioinspired robots, several versions of Trevor were tested. A photograph of the experimental set-up is shown in Fig. 12. The last three body segments make the DEO that generates the necessary voltage signals driving the DEAs, the first three are simple slave DEAs. All functional DE components are integrated into the robot and consist of polymer materials and carbon. At the current state of development there are still three copper wires in the robot, connecting the three pairs of master and slave DEAs. This is because we had not developed a layering technology to enable carbon conductor crossings at the time these measurements were made. This topic will be addressed in the next version of the robot.

To drive it, Trevor is placed on a rail-like track (Fig. 12A), possessing a high voltage and ground rail made of copper tape. The rail serves a power supply and as guidance, since the robot cannot be steered at the current state of development. The position of the robot is registered by a laser distance sensor. To supply the robot with power, its 5 feet possess conductive traces made of silver paint that contact copper rails. The right foot of each segment connects with the ground rail, the left foot with the high voltage rail. The power supply is a single DC voltage of 3,000 V to 4,000 V.

Fig. 13 summarizes the experimental results for the first demonstrators. Fig. 13A-C show the actuation of the three DEO actuators during one oscillation cycle. The yellow flashes illustrate an actuator having its maximum voltage at the depicted moment. The measured voltage signals and the input voltage for one demonstrator are shown in Fig. 13D. The low voltage levels of the signals do not reach voltages as low as those for free oscillators. This effect can be seen in all measurements. We believe that this is due to the added feet and friction forces that prevent the DEAs reaching their maximum elongation and, hence, the DESs their minimum resistance. However, the ratio between high and low signal levels is sufficient to generate a crawling motion of the robot. Fig. 13F depicts the motion of a demonstrator robot over time. Depending on the applied voltage the speed of the robot can be tuned. Higher voltages generate higher oscillation frequencies, more actuation within the single DEAs and more force. All three factors have positive feedback on the individual step size, frequency and, thus, the crawling speed of the robot.

Fig. 13E shows the already described influence of the series resistors on the frequency. The black line was measured using conventional high voltage resistors as reference. The single dots represent measurements using robots with integrated carbon resistors.

Discussion

The presented dielectric elastomer oscillator enables basic robotic structures that do not need conventional electronic components. They provide a contribution to the ongoing development of soft, electronics-free, biomimetic robotics that fulfill basic tasks. In the case of our demonstrator robot, Trevor, a crawling motion along a rail has been demonstrated, generated without any external control, conventional electronics or signal processing units. The movement of each DEA muscle is controlled by the mechanical strain of its neighbor, with strain coupled DES providing a "nervous system" that communicates both signal and excitatory charge for actuation, in a self-regulating system, inspired by live caterpillars.

The results show that it is possible to design biomimetic robots with actuators and charge control devices that are composed entirely of polymeric soft materials and without conventional, stiff,

electronic components. There is a vast number of promising studies focusing on the development of soft and smart structures and impetus concepts (e.g. *36*). Our investigations accelerate the development of fully soft, animal-like, robots without any rigid materials. All materials are suitable for modern production technologies such as 3D-, screen-, or ink jet-printing.

Besides the basic concept of using DEOs for the development of bioinspired robots, the general characteristics of DEOs with tunable frequency have been discussed. Measurements have shown that the frequency of individual oscillators can be tuned within a small range by changing the input voltage and within a wide range by changing the used series charging resistors. At the moment, variable carbon resistors, tunable by strain and a DE input voltage, are being developed. Those components enable an on-the-fly control of oscillation frequency and crawling speed of such robots.

Acknowledgement:

This project has received funding from the European Union's Horizon 2020 research and innovation
programme under the Marie Sklodowska-Curie grant agreement No 706754. This work was supported by a fellowship within the Postdoc-Program of the German Academic Exchange Service (DAAD). We wish to thank Benjamin M. O'Brien for the concept of the oscillator-driven crawling robot and the helpful discussions we have had with him during the development of the final electronics-free prototype.

References:

1. K. Suzumori, S. Iikura, H. Tanaka, Applying a flexible microactuator to robotic mechanisms. *Control Systems, IEEE* **12**, 21-27 (1992).
2. C.-P. Chou, B. Hannaford, Measurement and modeling of McKibben pneumatic artificial muscles. *Robotics and Automation, IEEE Transactions on* **12**, 90-102 (1996).
3. R. F. Shepherd, F. Ilievski, W. Choi, S. A. Morin, A. A. Stokes, *et al.* Multigait soft robot. *Proceedings of the National Academy of Sciences* **108**, 20400-20403, (2011).
4. R. K. Katzschmann, A. D. Marchese, D. Rus, in *Experimental Robotics,* M. A. Hsieh, O. Khatib, V. Kumar Eds. (Springer International Publishing, Switzerland, 2016), chap 7, 405-420.
5. M. Calisti, M. Giorelli, G. Levy, B. Mazzolai, B. Hochner, *et al.* An octopus-bioinspired solution to movement and manipulation for soft robots. *Bioinspiration & biomimetics* **6**, 036002 (2011).
6. D. Rus and M. T. Tolley, Design, fabrication and control of soft robots. *Nature* **521**, 467-475 (2015)
7. C. Majidi, Soft robotics: a perspective—current trends and prospects for the future. *Soft Robotics* **1**, 5-11 (2014).
8. D. Trivedi, C. D. Rahn, W. M. Kier, I. D. Walker, Soft robotics: Biological inspiration, state of the art, and future research. *Applied Bionics and Biomechanics* **5**, 99-117 (2008).
9. J. A. Rogers, T. Someya, Y. Huang, Materials and mechanics for stretchable electronics. *Science* **327**, 1603-1607 (2010).
10. B. Mosadegh, C.-H. Kuo, Y.-C. Tung, Y.-s. Torisawa, T. Bersano-Begey, H. Tavana and S. Takayama, Integrated elastomeric components for autonomous regulation of sequential and oscillatory flow switching in microfluidic devices. *Nature physics* **6**, 433-437 *Nature Research,* (2010).
11. M. Wehner, M. T. Tolley, Y. Mengüç, Y.-L. Park, A. Mozeika, Y. Ding, C. Onal, R. F. Shepherd, G. M. Whitesides and R. J. Wood, Pneumatic Energy Sources for Autonomous and Wearable Soft Robotics. *Soft Robotics* **1**, 263-274 *Mary Ann Liebert Inc,* (2014).
12. M. Wehner, R. L. Truby, D. J. Fitzgerald, B. Mosadegh, G. M. Whitesides, J. A. Lewis and R. J. Wood, An integrated design and fabrication strategy for entirely soft, autonomous robots. *Nature* 536, 451-455 Springer Nature, (2016).
13. Carpi, F.; de Rossi, D. E.; Kornbluh, R.; Pelrine, R. & Sommer-Larsen, P. (Eds.) *Dielectric Elastomers as Electromechanical Transducers: Fundamentals, Materials, Devices, Models and Applications of an Emerging Electroactive Polymer*. (Elsevier, Amsterdam, 2008).
14. I. A. Anderson, T. A. Gisby, T. G. McKay, B. M. O'Brien, E. P. Calius, Multi-functional dielectric elastomer artificial muscles for soft and smart machines. *Journal of Applied Physics* **112**, 041101 (2012).
15. K. J. Kim (Ed.) Electroactive polymers for robotic applications: Artificial muscles and sensors. Springer, (2007).

16. R. Pelrine, R. Kornbluh, Q. Pei, J. Joseph, High-Speed Electrically Actuated Elastomers with Strain Greater Than 100%. *Science* **287**, 836-839 (2000).
17. T. Li, C. Keplinger, R. Baumgartner, S. Bauer, W. Yang, Z. Suo, Giant voltage-induced deformation in dielectric elastomers near the verge of snap-through instability. *Journal of the Mechanics and Physics of Solids* **61**, 611-628 (2012).
18. Y. Bar-Cohen, Electroactive polymers as artificial muscles: A review. *Journal of Spacecraft and Rockets* **39**, 822-827 (2002).
19. L. A. Toth, A. A. Goldenberg, Control system design for a dielectric elastomer actuator: the sensory subsystem. *Proc. SPIE* **4695**, 323-334 (2002).
20. C. Keplinger, M. Kaltenbrunner, N. Arnold, S. Bauer, Capacitive extensometry for transient strain analysis of dielectric elastomer actuators. Applied Physics Letters 92, 192903 (2008).
21. B. O'Brien, T. Gisby, I. A. Anderson, Stretch sensors for human body motion. *Proc. SPIE* **9056**, 905618 (2014).
22. T. McKay, B. O'Brien, E. Calius and I. Anderson, Self-priming dielectric elastomer generators. *Smart Materials and Structures* **19**, 055025 (2010).
23. I. A. Anderson, P. Illenberger and B. M. O'Brien, Energy harvesting for dielectric elastomer sensing. *Electroactive Polymer Actuators and Devices (EAPAD) 2016*, SPIE-Intl Soc Optical Eng, (2016).
24. T. Gisby, B. O'Brien, I. A. Anderson, in *Electroactivity in Polymeric Materials*, Lenore Rasmussen Ed. (Springer US, 2012) pp. 131-141.
25. A. Poulin, S. Rosset and H. R. Shea, Printing low-voltage dielectric elastomer actuators. Applied Physics Letters 107, 244104 (2015).
26. F. M. Weiss, T. Töpper, B. Osmani, S. Peters, G. Kovacs and B. Müller, Electrospraying Nanometer-Thin Elastomer Films for Low-Voltage Dielectric Actuators. Advanced Electronic Materials 2, 1500476 (2016).
27. F. B. Madsen, L. Yu, A. E. Daugaard, S. Hvilsted and A. L. Skov, Silicone elastomers with high dielectric permittivity and high dielectric breakdown strength based on dipolar copolymers . Polymer 55, 6212 - 6219 (2014).
28. D. Beruto, M. Capurro, G. Marro, Piezoresistance behavior of silicone--graphite composites in the proximity of the electric percolation threshold. *Sensors and Actuators A: Physical* **117**, 301-308 (2005).
29. B. M. O'Brien, E. P. Calius, T. Inamura, S. Q. Xie, I. A. Anderson, Dielectric elastomer switches for smart artificial muscles. *Applied Physics A* **100**, 385-389 (2010).
30. B. M. O'Brien, I. A. Anderson, An artificial muscle ring oscillator. *Mechatronics, IEEE/ASME Transactions on* **17**, 197-200 (2012).
31. K. E. Wilson, E.-F. M. Henke, G. A. Slipher and I. A. Anderson, Rubbery logic gates. *Extreme Mechanics Letters* **9**, 188 - 194 (2016).
32. M. Mandal and B. Sarkar, Ring oscillators: Characteristics and applications. *Indian journal of pure & applied physics* **48**, 136-145 (2010).

33. C. C. Foo, S. J. A. Koh, C. Keplinger, R. Kaltseis, S. Bauer and Z. Suo, Performance of dissipative dielectric elastomer generators. *Journal of Applied Physics* **111**, 094107 (2012).
34. S. Michel, X. Q. Zhang, M. Wissler, C. Löwe and G. Kovacs, A comparison between silicone and acrylic elastomers as dielectric materials in electroactive polymer actuators. *Polymer International* **59**, 391-399 (2010).
35. L. I. van Griethuijsen, B. A. Trimmer, Locomotion in caterpillars *Biological Reviews* **89**, 656-670 (2014).
36. N. W. Bartlett, M. T. Tolley, J. T. B. Overvelde, J. C. Weaver, B. Mosadegh, *et al.* A 3D-printed, functionally graded soft robot powered by combustion. *Science* **349**, 161-165 (2015).

Supplementary Material

Movie S1

This Movie shows the movement of the actual version of the robot without any conventional electronics, emphasizing the signal generation unit and the movement of the feet. https://youtu.be/YF21b4a6d7g

Movie S2

The movie shows and explains the designed robot in an earlier version, still containing conventional resistors. However, it gives an impression of the biologically-inspired movement generated by the dielectric elastomer actuator and switch network. The movie was produced for promotional purposes related to the Dielectric Elastomer Switch technology. https://youtu.be/QmfurTfRyKU

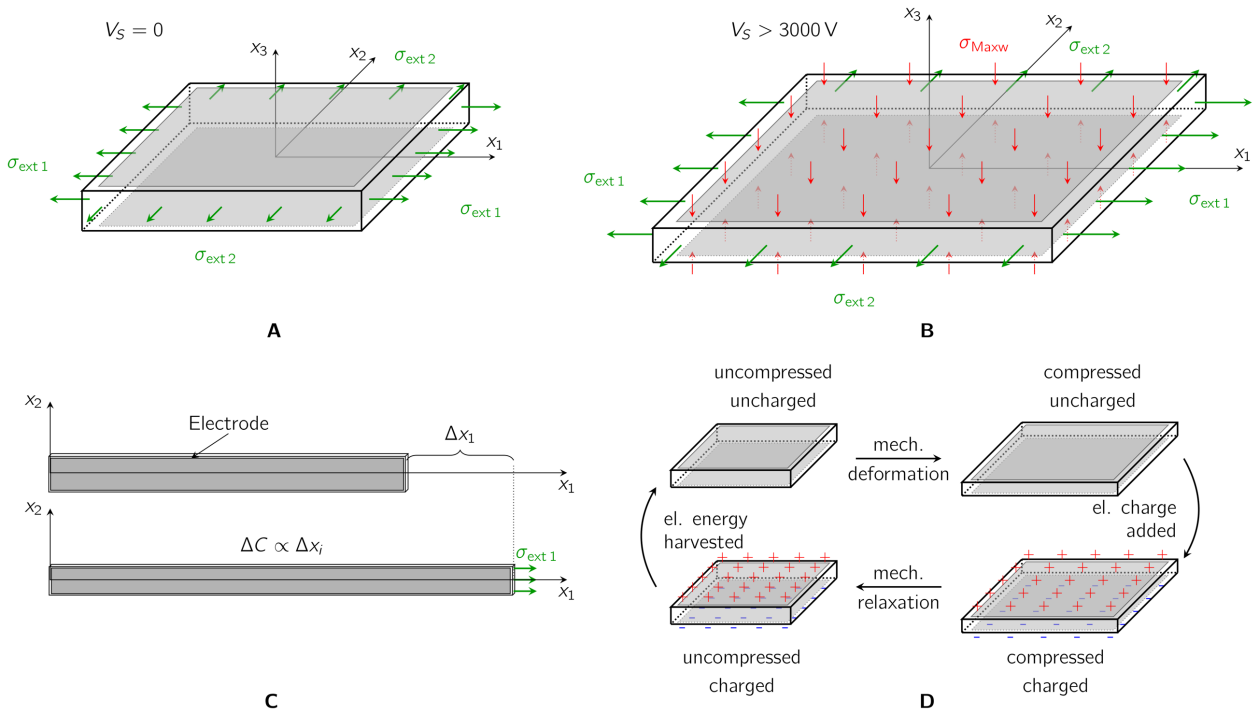

Fig. 1 Dielectric Elastomer Actuator as multifunctional material. (A) DEA membrane equibiaxially pre-strained by the external stresses $\sigma_{ext\,i}$. There is no supply voltage V_S applied to the compliant electrodes. (B) A suitable supply voltage V_S (typically > 3000 V) is applied to the compliant electrodes. That causes a Maxwell pressure σ_{Maxw} along the thickness of the membrane. According to the governing equations the DEA will be compressed in x_3-direction and elongate in direction x_1 and x_2. Combining such an DEA with a flexible mechanical structure makes an actuator. (C) A DE stretch sensor for large stretches. Straining the DE causes the length, width and thickness and, therefore, the capacitance C to change. External electronics can measure the strain from the changing capacitance. (D) A DE generator converting mechanical deformation energy into electrical energy which can be harvested.

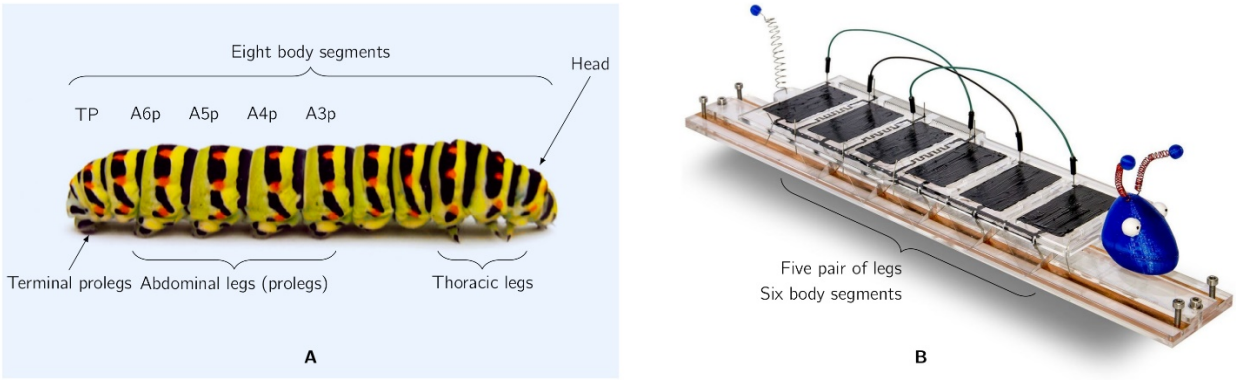

Fig. 2 The caterpillar as biological inspiration for a crawling locomotion robot without conventional electronics. (A) Structure of a live caterpillar consisting of eight body segments. The first three possess thoracic legs, the 3rd to 6th abdominal legs – the so-called prolegs - and the last the terminal prolegs. (B) "Trevor" the biomimetic, electronic-free crawling locomotion robot comprises six body segments and five pairs of legs.

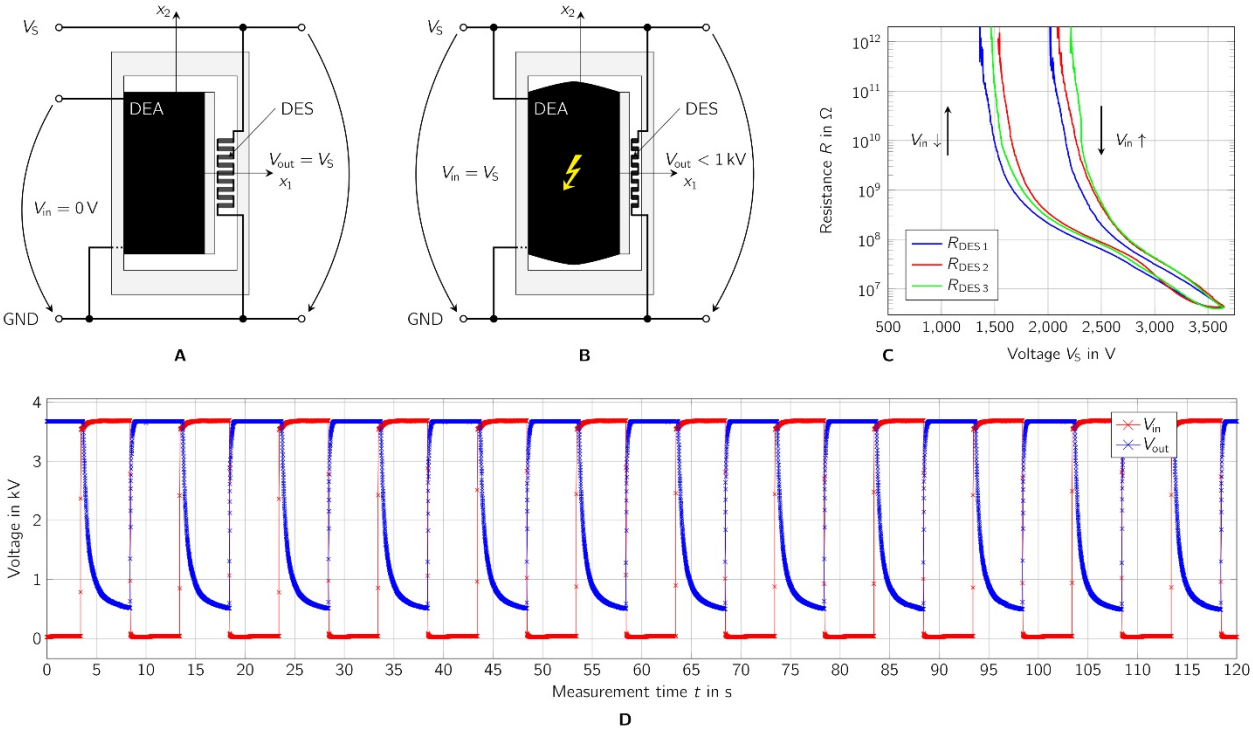

Fig. 3 Dielectric elastomer inverter. DE inverter in its OFF state (A) and in its ON state (B). Depending on the level of input voltage, the inverter will change its output resistance by more than five orders of magnitude and, therefore, its output voltage level (C). Upon a changing input signal between high and low the inverter will always calculate the inverse of its input; measurement results show in (D).

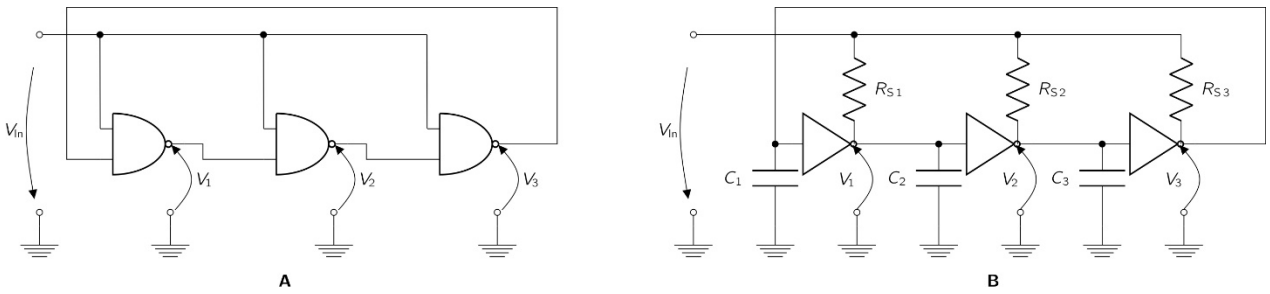

Fig. 4 Dielectric elastomer oscillators. (A) NAND based design according to O'Brien (*30*). (B) new design with reduced complexity and charging resistors to set the oscillation frequency.

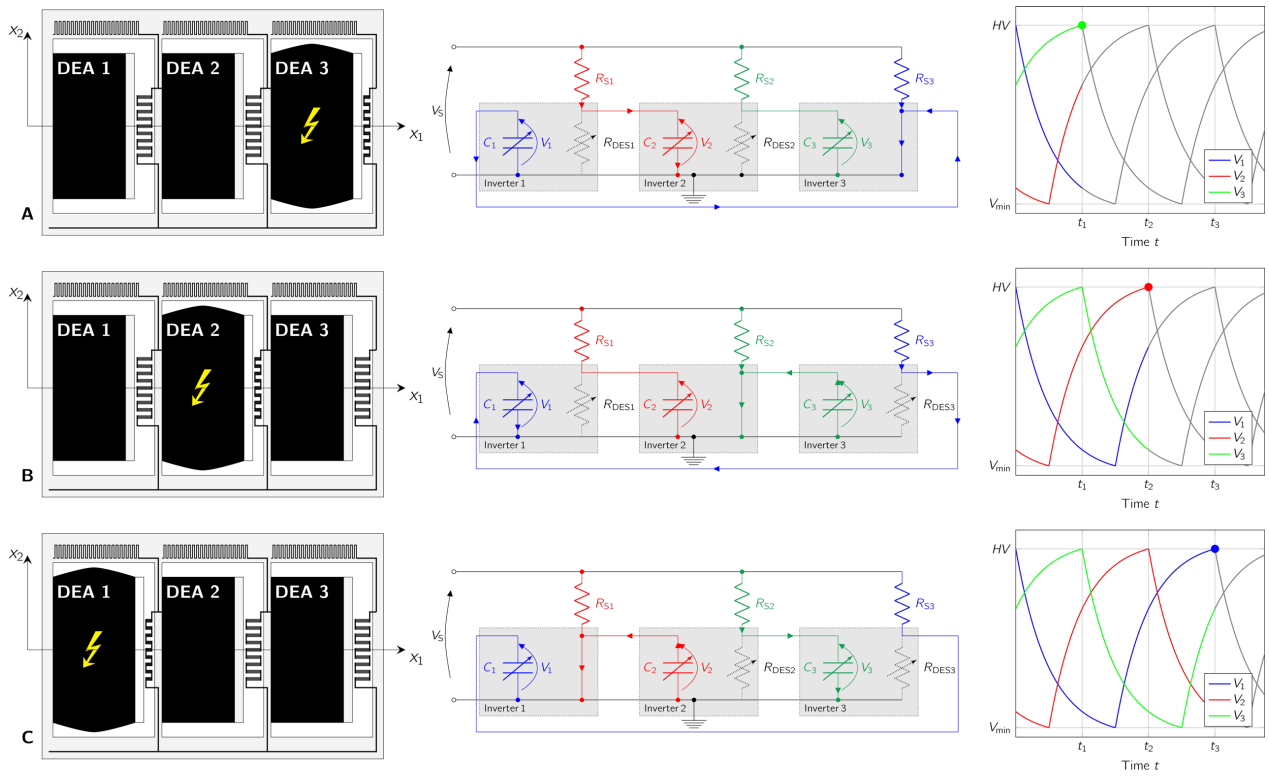

Fig. 5 Idealized signal generation in a DEO at different times t_i during one oscillation cycle. (Left) schematic, idealized elongation of DEAs, (middle) actual electrical circuit condition, (right) idealized voltage signals at moment t_i: (A) moment t_1, DEA 1 discharging, DEA 2 charging, DEA 3 completely charged, DES 1 and DES 2 not conducting, DES 3 conducting; (B) moment t_2, DEA 1 charging, DEA 2 completely charged, DEA 3 discharging, DES 1 not conducting, DES 2 conducting, DES 3 not conducting; (C) moment t_3, DEA 1 completely charged, DEA 2 discharging, DEA 3 charging, DES 1 conducting, DES 2 and DES 3 not conducting.

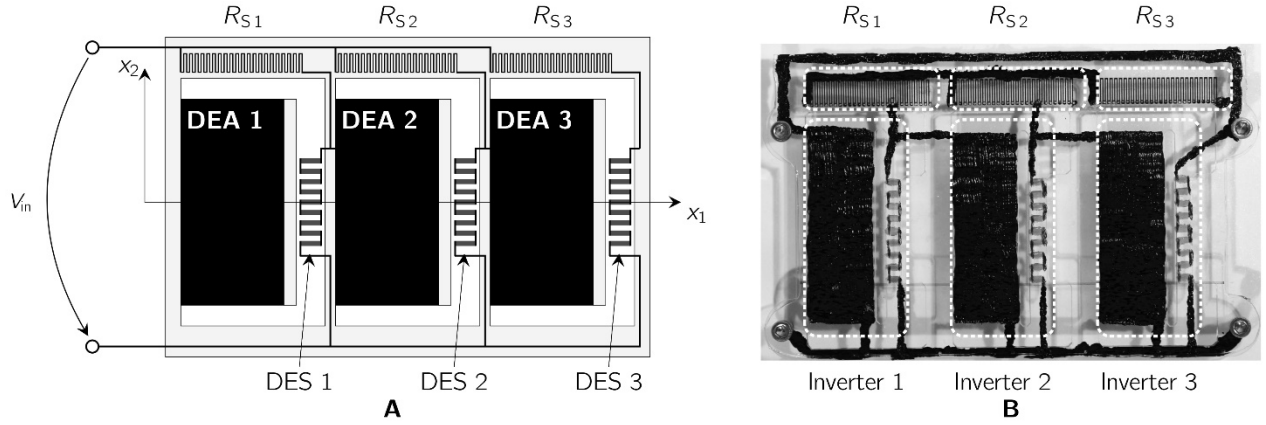

Fig. 6 Dielectric elastomer oscillator. (A) Schematic representation of a DEO possessing three DEA-DES subunits, representing a closed-loop, series connection of three DE inverters and three series resistors R_S controlling the oscillation frequency. (B) photograph of an example DEO consisting of three inverters and three series resistors. All necessary DE components are assembled on a single DE membrane supported by a 3mm PMMA frame.

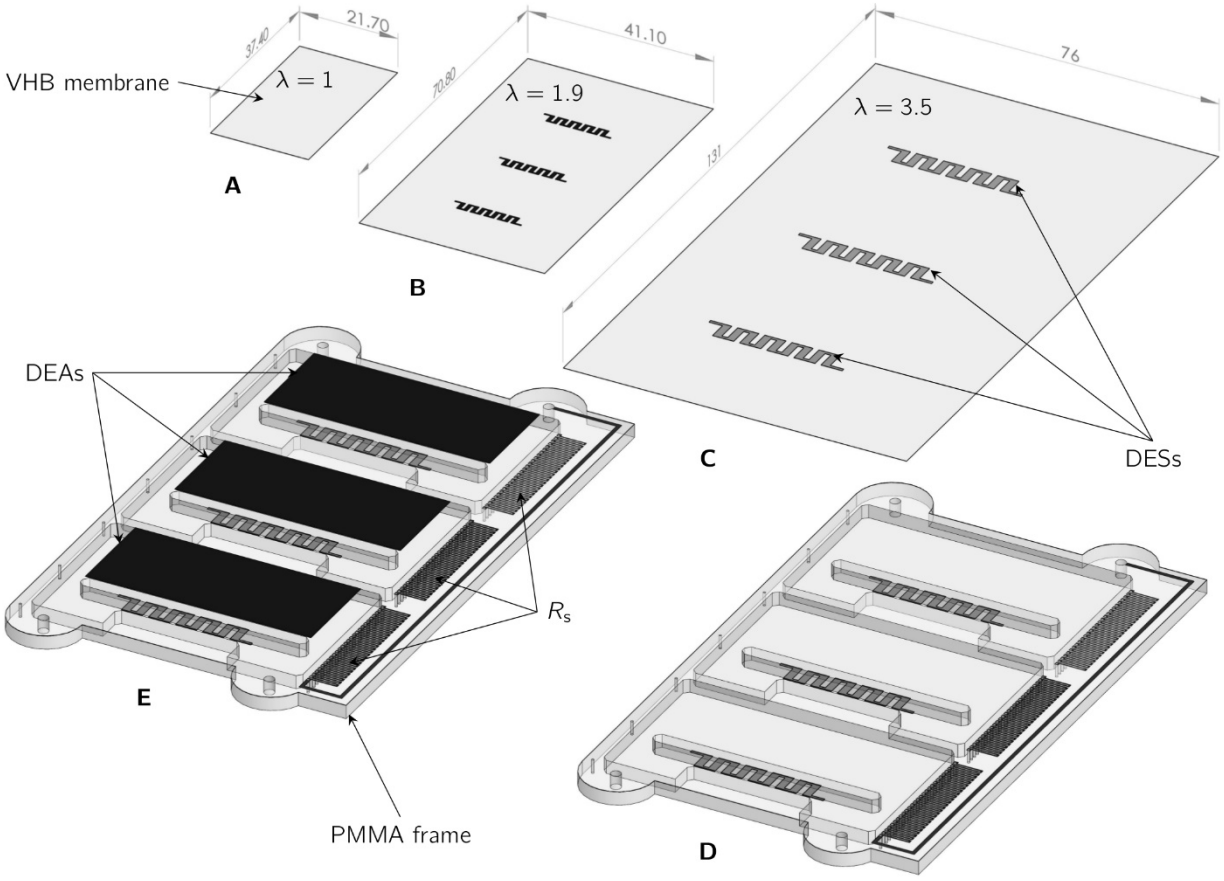

Fig. 7 Production steps of DEOs. (A) An unstrained VHB membrane is pre-strained by λ=1.9 in both directions, and the DES are imprinted using a PDMS stamp and carbon grease (B). To enable switching the membrane is further pre-strained to a final equi-biaxial pre-strain of λ=3.5. A 3 mm thick, laser cut, PMMA frame, that already carries the series resistors R_s, is glued to the membrane and cut loose (D). Finally, in (E), the DEA electrodes are applied to the membrane and the necessary carbon grease connections are applied (not shown here).

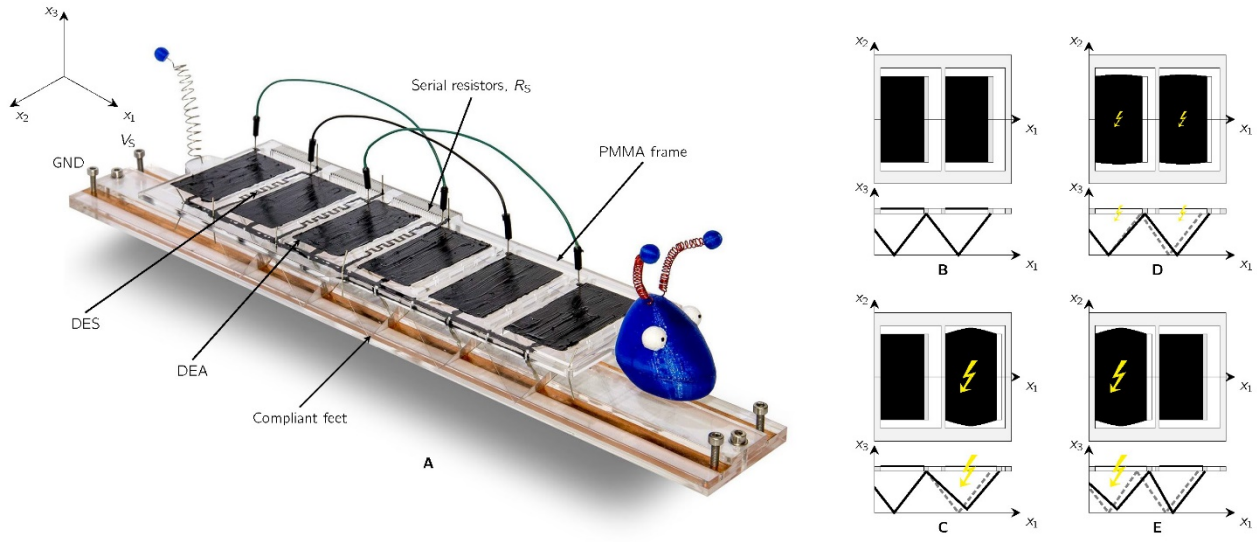

Fig. 8 Robot design and principle of operation. (A) Photograph of the demonstrator robot – Trevor the Caterpillar – containing no conventional electronic parts. All functional elements consist of DE structures (DEAs and DES) and imprinted carbon resistors. **(B)** Model of the robot's movement. The in-plane electromechanical traveling wave

generated within the robot's DE network is translated into a forward motion by its flexible legs, which simultaneously connect the robot to its driving voltage and the surface.

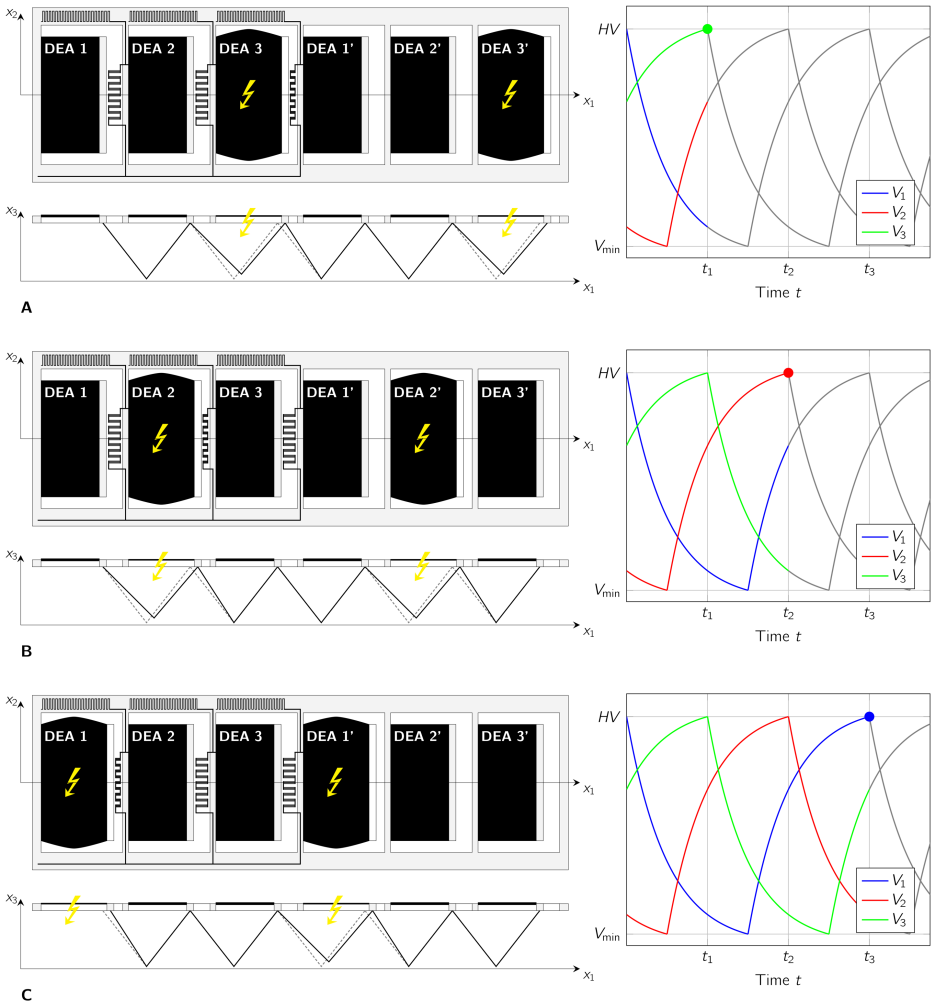

Fig. 9 Schematic functionality of the crawling electronics-free robot. The electromechanical wave travels from the right to the left end of the robot. (A) at time t_1 the voltage V_3 over DEA 3 and DEA 3' reaches its maximum value, both actuators elongate, the membrane loses tension and the connected feet are lifted and moved forward. (B) At t_2 V_2 reaches its maximum. The corresponding DEAs elongate and move the connected feet, the feet of the step before are lowered and connected to the surface again. At t_3 DEA 3 and DEA 3' are activated (C). Afterwards, the whole cycle starts from its beginning.

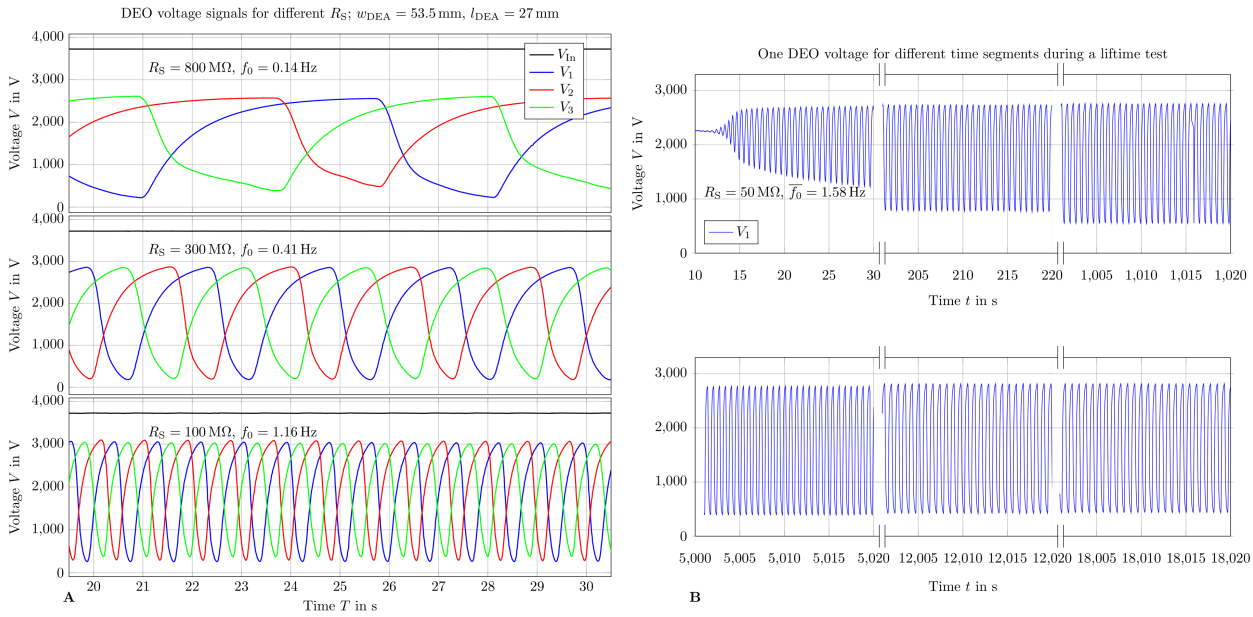

Fig. 10 Measured voltage signals for an example DEO. (A) **Measured signal waveforms for** different series charging resistors R_S. The frequency of the three voltage oscillations can be controlled by the value of series resistors. (B) Lifetime measurement: depiction of measured signal waveforms for different time sections of a long time experiment.

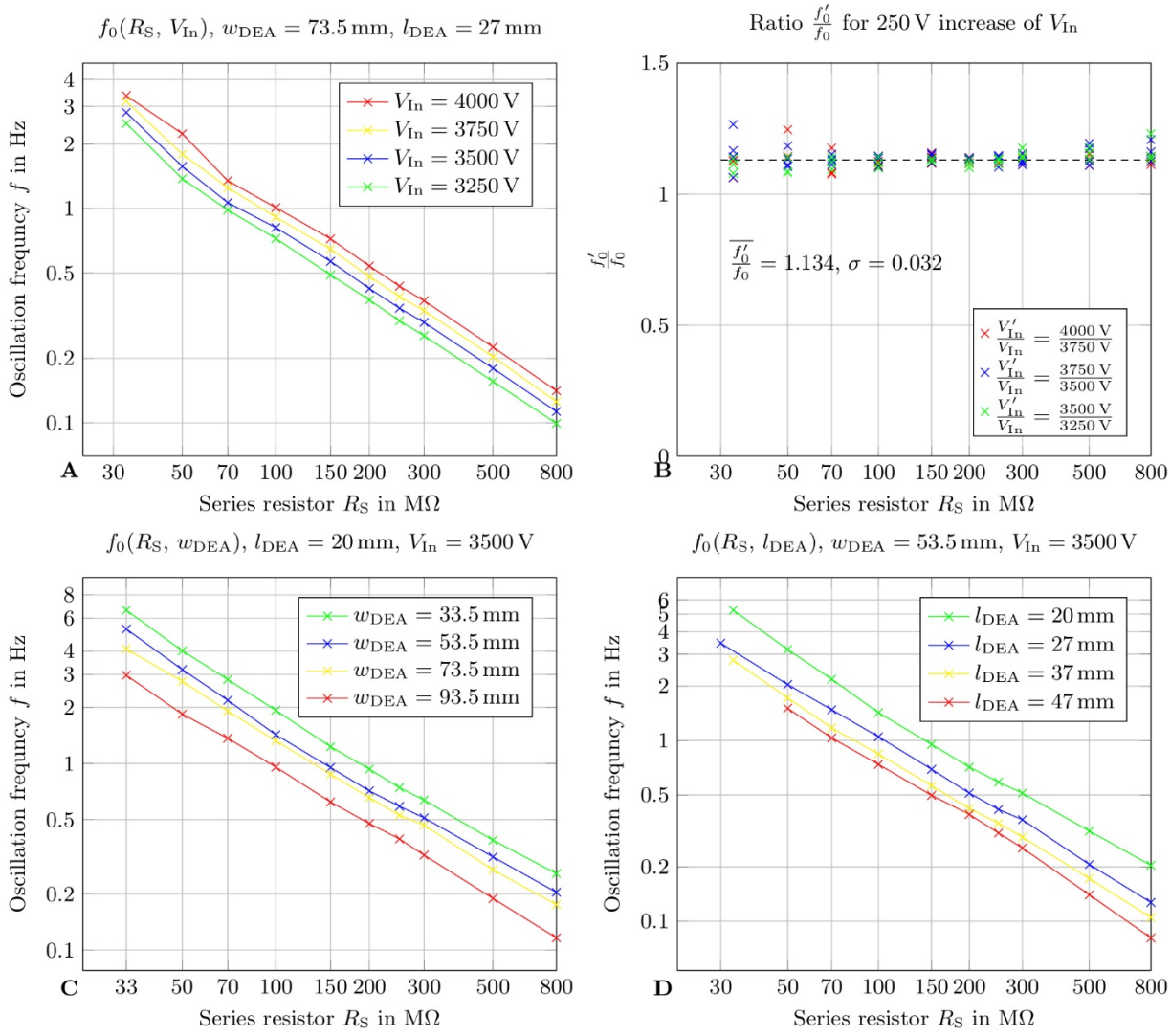

Fig. 11 Frequency of oscillating voltages generated by DEOs from a single DC input voltage. In general, the oscillation frequency depends on the value of the series charging resistors R_S. (A) depicts the voltage dependence of the frequency. The higher the input voltage V_{In}, the higher the frequency f_0. A rise of 250V increases the oscillation frequency by 13.4% on average (B). Furthermore, the frequency depends on the area of the DEA, represented by the width dependence (C) and the length dependence (D).

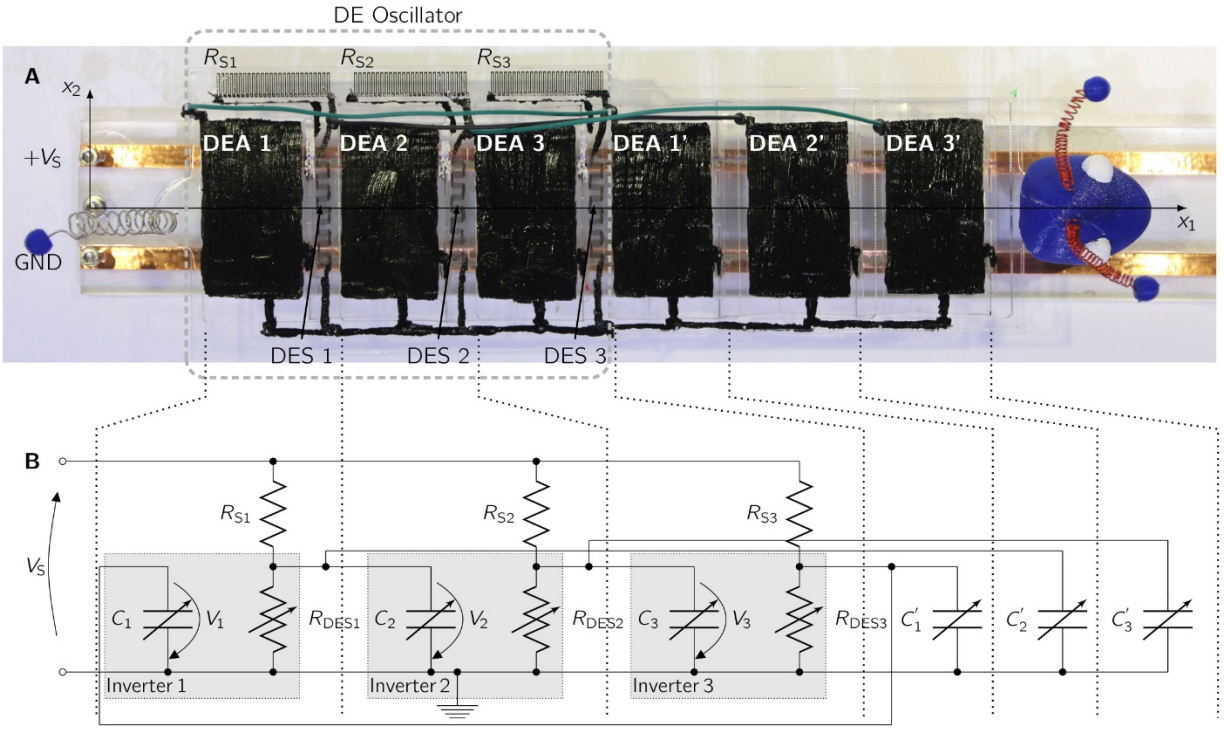

Fig. 12 Bioinspired crawling electronics free robot – Trevor the caterpillar. (A) Photograph of the robot from above and (B) electrical model, depicting all dielectric elastomer electronic components, being the series charging resistors R_{Si}, six dielectric elastomer actuators DEA i and their corresponding capacitances C_i, three dielectric elastomer switches DES i and their corresponding variable resistors R_{DESi}.

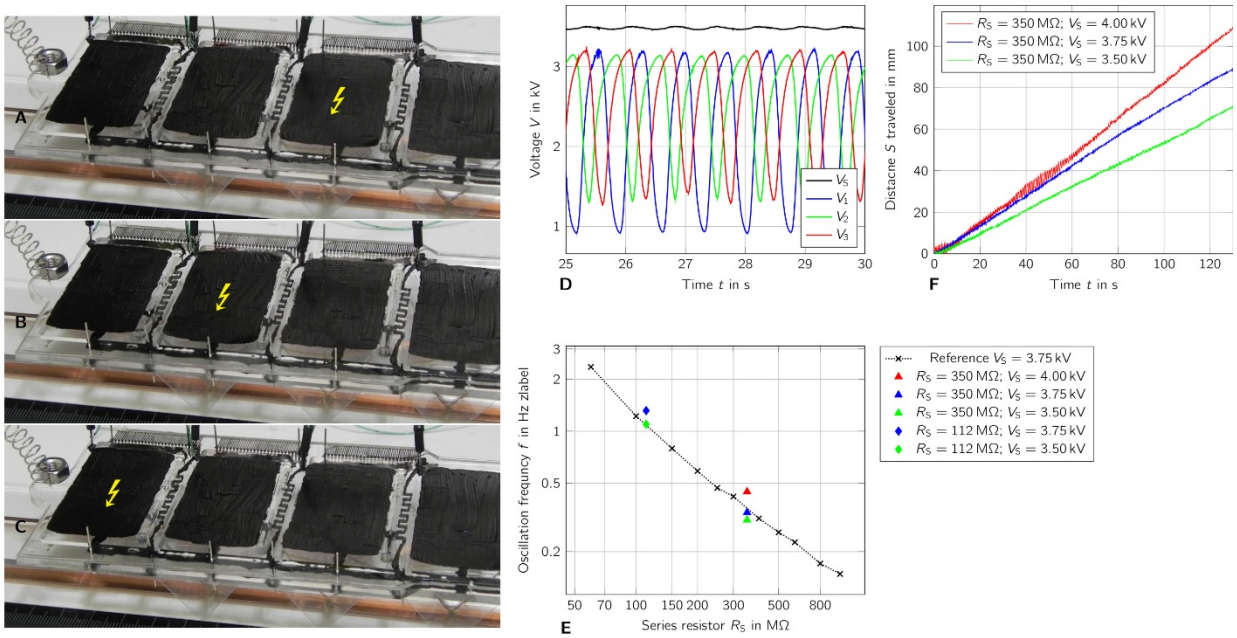

Fig. 13 Experimental results for the electronic-free soft robot. (A-C) Traveling high-voltage waveform along the robot's DE muscles and resulting compression of the corresponding DESs - flash symbols mark position of the highest voltage at each time period. **(D)** Measured oscillating voltage signals according to the nomenclature of (Fig. 12B/C). **(E)** Influence of series resistor values R_{Si} and the supply voltage V_S on the oscillation frequency of the electromechanical wave. **(F)** Measured position for the robot during experiment for different supply voltages V_S.